Lopez et al., http://www.jgp.org/cgi/content/full/jgp.201210983/DC1

Characterization of hCx26 hemichannel currents

Xenopus oocytes are well suited for study of connexin hemichannels because they show robust currents from heterologously expressed connexins and, because of their large cytoplasmic volume, they can tolerate and recover from substantial hemichannel opening. Previous reports have shown that large depolarizing pulses and low extracellular Ca^{2+} concentrations activate Cx26 hemichannels (Ripps et al., 2004; González et al., 2006; Sánchez et al., 2010). However, precautions must be taken to guard against contaminating currents arising from an endogenous connexin (Cx38), voltage-activated Na^+ channels (activated above 20 mV), and Ca^{2+}-activated Cl^- channels. Currents from these endogenous channels can mask hCx26 hemichannel currents and complicate quantitative gating analysis (Ebihara, 1996; Ripps et al., 2002a,b; Sánchez et al., 2010). Here, we describe studies to identify the distinctive gating properties of hCx26 hemichannels using the two-electrode voltage-clamp technique to allow for the study of hemichannel regulation by external Ca^{2+}. The activation of the endogenous Na^+ channels can be avoided by restricting depolarizations to 0 mV. Thus, we first examined the current responses elicited by a depolarizing pulse from −80 to 0 mV, but with different durations. Fig. S1 A shows that the peak tail current magnitude is a function of the duration of the depolarizing pulse rather than the magnitude of the current activated during the depolarization. Maximal tail current activation is reached after depolarizing pulses of ∼40 s (Fig. S1 B). This suggests that channel activation by a depolarizing pulse may be kinetically complicated, like that of HERG channels (Schönherr and Heinemann, 1996; Smith et al., 1996; Spector et al., 1996). Similar to analysis of HERG channels, we used the peak tail currents to assess hCx26 current activation. Fig. S1 C shows the differences between the currents activated by depolarizing pulse from −80 to 0 mV from oocytes expressing hCx26 compared with oocytes injected only with antisense against Cx38, the endogenous connexin expressed by *Xenopus* oocytes. Note the prominent activation of outward connexin hemichannel currents and the corresponding tail currents only when cRNA for hCx26 is injected.

Large depolarizing voltages and Ca^{2+} influx through hCx26 hemichannels can evoke endogenous Cl^- currents in *Xenopus* oocytes (Sánchez et al., 2010). We first assessed Ca^{2+}-activated Cl^- currents in oocytes expressing hCx26 that were treated with the 10 µM Ca^{2+} ionophore ionomicyn in 0.01 mM of extracellular Ca^{2+} Ringer's solution, and then exposed to 10 mM Ca^{2+}. Fig. S2 A shows an example of an ionomicyn-treated oocyte held at −80 mV. At 0.01 mM Ca^{2+}, a stable leak current is observed. Switching to 10 mM Ca^{2+} elicits a prominent inward current followed by recovery. The prominent inward current corresponds to opening of Ca^{2+}-activated Cl^- channels, as described by others (Hartzell et al., 2005). Conversely, oocytes injected with 120 µM BAPTA show a lack of inward currents under these conditions (Fig. S2 B). We also evaluated whether Ca^{2+}-activated Cl^- currents can be triggered by the opening of hCx26 hemichannels after depolarizing pulses (caused by Ca^{2+} entry through the hemichannels). Fig. S2 C shows tail currents with multiphasic deactivations after repolarizing from voltages >20 mV. However, oocytes injected with 120 µM BAPTA showed only monotonic deactivation kinetics of tail currents, with single-exponential fits of ∼12 s (Fig. S2 D, red lines). This indicates that enhanced opening of hemichannels promotes Ca^{2+}-activated Cl^- currents, and that 120 µM BAPTA is sufficient to eliminate these currents. Importantly, we consistently observed that depolarizing pulses from −80 to 0 mV along with moderate levels of expression of hCx26 generate tail currents with single-exponential decays of ∼12 s, indicating that the tail currents reflect deactivation only of hCx26 hemichannels, without contamination by other deactivating currents. Because of the reliability and reproducibility of tail currents obtained with this protocol, we performed steady-state and kinetic studies of tail currents in response to changes in external Ca^{2+} concentration. Even so, injections with 120 µM BAPTA were applied in some cases when oocytes expressed high levels of hCx26 currents and when the mutant hemichannel currents were exposed to high extracellular Ca^{2+} (≥3.5 mM).

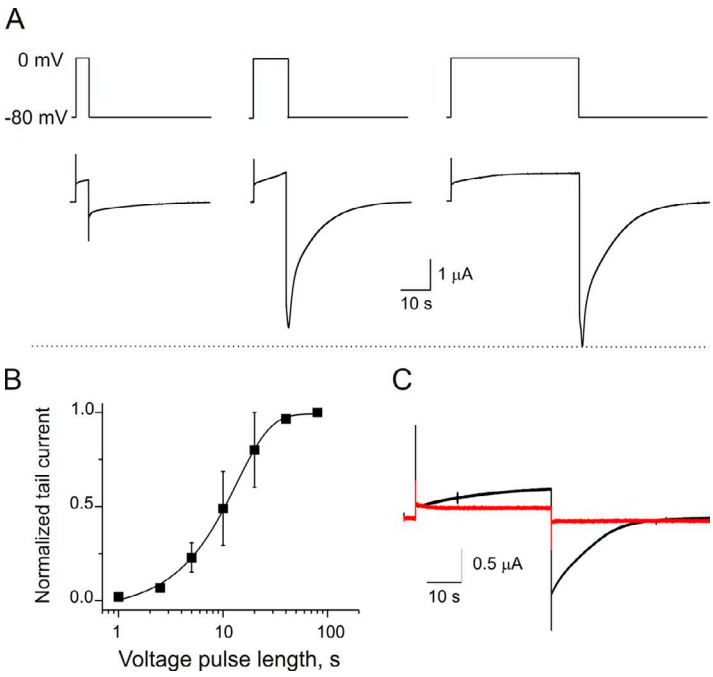

Figure S1. hCx26 hemichannel currents. (A) Currents elicited in response to voltage steps from −80 to 0 mV from oocytes expressing mRNA for hCx26 in the presence of 1.8 mM of external Ca^{2+}. Pulses of 5, 10, and 40 s show that tail current magnitude is a function of the duration of the depolarizing pulse. (B) Normalized tail currents in response to voltage pulses from −80 to 0 mV of different durations. The data points represent mean ± SEM of at least three independent measurements. (C) Comparison of currents in the presence of 1.8 mM Ca^{2+} elicited by a voltage pulse from −80 to 0 mV from oocytes injected with both hCx26 mRNA and Cx38 antisense (black) or only with Cx38 antisense (red).

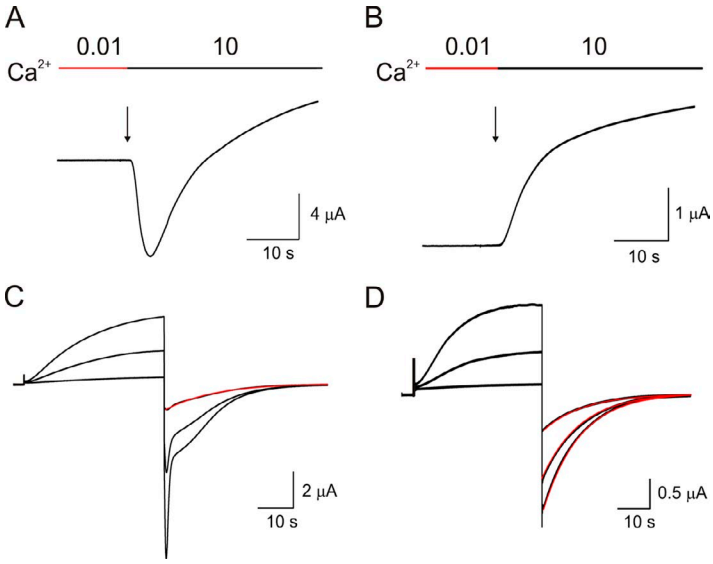

Figure S2. Distinguishing gating properties of hCx26 hemichannels from endogenous Ca^{2+}-activated chloride currents. (A and B) Oocytes expressing hCx26 hemichannels were treated with 10 µM ionomicin in the presence of 0.01 mM of extracellular Ca^{2+} Ringer's solution, and then exposed to 10 mM Ca^{2+}. A large inward current mediated by Ca^{2+}-activated chloride channels is observed (A), but not when the oocyte was previously injected with 120 µM BAPTA (B). (C and D) Depolarizing voltage pulses from −80 to 0, 20, and 40 mV elicited currents from oocytes expressing hCx26 hemichannels in the presence of 1.8 mM of extracellular Ca^{2+}. The tail currents display multiple kinetic components after depolarizing pulses of 20 and 40 mV (C). Conversely, with prior injection of the oocyte with 120 µM BAPTA, only monotonic deactivation kinetics of tail currents are seen (D). Red lines correspond to single-exponential fitting of the tail currents.

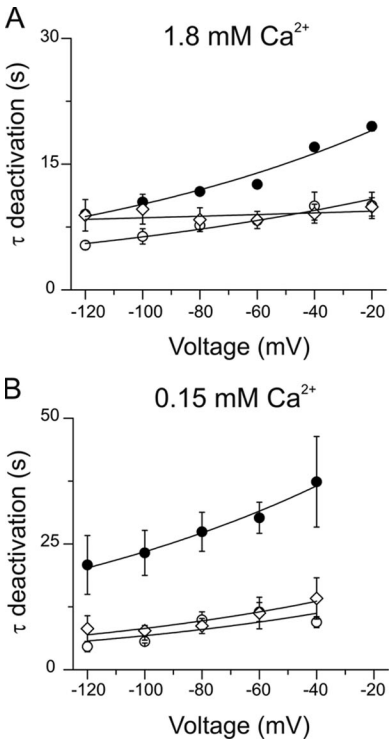

Figure S4. Deactivation kinetics are only modestly modulated by voltage in wild-type and D50N/Y mutant hemichannels. (A) Deactivation time constants for oocytes expressing wild-type (closed circles), D50N (open circles), and D50Y (slow component; open diamonds) mutant hemichannels were obtained in the presence of 1.8 mM Ca^{2+} after a voltage step from 0 mV to different voltage steps (−120 to −20 mV). The solid lines are fits to the data using an equation of the form: $\tau_{deactivation} = A \exp(-zV/RT)$, where A is a constant, z defines the voltage dependence of $\tau_{deactivation}$, and V is the voltage. Parameters z were 0.2 ± 0.02, 0.17 ± 0.01, and 0.03 ± 0.02 for the wild-type, D50N, and D50Y mutants, respectively. (B) Deactivation time constants for wild-type and D50N/Y mutant hemichanels in the presence of 0.15 mM of extracellular Ca^{2+}, as described in A. Parameters z were 0.21 ± 0.1, 0.2 ± 0.04, and 0.19 ± 0.01 for the wild-type, D50N, and D50Y mutants, respectively.

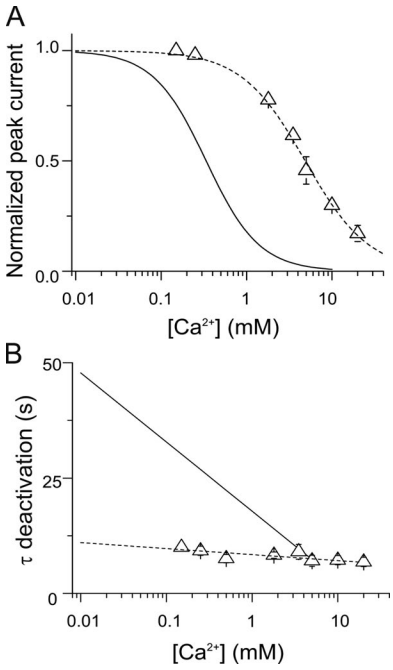

Figure S3. Ca^{2+} regulation in D50C mutant hemichannels. (A) Ca^{2+} dose–response relation for oocytes expressing D50C mutant hemichannels estimated from the peak tail current after a voltage pulse from −80 to 0 mV. The solid and dotted lines represent the best fits to a Hill equation for wild-type (from Fig. 1 B) and D50C mutant hemichannels, respectively. (B) Deactivation time constants as a function of Ca^{2+} concentration. Dotted lines are the best linear fit to the D50N/Y mutant hemichannel data. The solid line corresponds to the linear fit of the average data for wild-type hemichannels (from Fig. 1 C). The data points represent mean ± SEM of at least three independent measurements.

REFERENCES

Ebihara, L. 1996. Xenopus connexin38 forms hemi-gap-junctional channels in the nonjunctional plasma membrane of Xenopus oocytes. *Biophys. J.* 71:742–748. http://dx.doi.org/10.1016/S0006-3495(96)79273-1

González, D., J.M. Gómez-Hernández, and L.C. Barrio. 2006. Species specificity of mammalian connexin-26 to form open voltage-gated hemichannels. *FASEB J.* 20:2329–2338. http://dx.doi.org/10.1096/fj.06-5828com

Hartzell, C., I. Putzier, and J. Arreola. 2005. Calcium-activated chloride channels. *Annu. Rev. Physiol.* 67:719–758. http://dx.doi.org/10.1146/annurev.physiol.67.032003.154341

Ripps, H., H. Qian, and J. Zakevicius. 2002a. Blockade of an inward sodium current facilitates pharmacological study of hemi-gap-junctional currents in Xenopus oocytes. *Biol. Bull.* 203:192–194. http://dx.doi.org/10.2307/1543391

Ripps, H., H. Qian, and J. Zakevicius. 2002b. Pharmacological enhancement of hemi-gap-junctional currents in Xenopus oocytes. *J. Neurosci. Methods.* 121:81–92. http://dx.doi.org/10.1016/S0165-0270(02)00243-1

Ripps, H., H. Qian, and J. Zakevicius. 2004. Properties of connexin26 hemichannels expressed in Xenopus oocytes. *Cell. Mol. Neurobiol.* 24:647–665. http://dx.doi.org/10.1023/B:CEMN.0000036403.43484.3d

Sánchez, H.A., G. Mese, M. Srinivas, T.W. White, and V.K. Verselis. 2010. Differentially altered Ca^{2+} regulation and Ca^{2+} permeability in Cx26 hemichannels formed by the A40V and G45E mutations that cause keratitis ichthyosis deafness syndrome. *J. Gen. Physiol.* 136:47–62. http://dx.doi.org/10.1085/jgp.201010433

Schönherr, R., and S.H. Heinemann. 1996. Molecular determinants for activation and inactivation of HERG, a human inward rectifier potassium channel. *J. Physiol.* 493:635–642.

Smith, P.L., T. Baukrowitz, and G. Yellen. 1996. The inward rectification mechanism of the HERG cardiac potassium channel. *Nature.* 379:833–836. http://dx.doi.org/10.1038/379833a0

Spector, P.S., M.E. Curran, A. Zou, M.T. Keating, and M.C. Sanguinetti. 1996. Fast inactivation causes rectification of the IKr channel. *J. Gen. Physiol.* 107:611–619. http://dx.doi.org/10.1085/jgp.107.5.611